International Journal of
Electrical Machines & Drives

Volume 8, Issue 2, 2022
DOI (Journal): 10.37628/IJEMD

http://ecc.journalspub.info/index.php?journal=JEMD&page=index

Research IJEMD

# The Structure Optimization Design of Bearingless Switched Reluctance Motor for Flywheel Energy Storage

Huiqin Sun[1,]*, Sifei Wang[2], Wanqing Zhang[2], Chengran Mei[2], Zheng Tian[2], Chunzhi Shi[2]

***Abstract***

*In order to optimize the torque performance of high-speed Bearingless Switched Reluctance Motor (BSRM) for flywheel energy storage and solve the problem of large torque ripple caused by the double salient motor structure, based on the mathematical model of torque and radial force, this paper proposes helical teeth structure that can reduce the torque ripple during commutation. Taking 12/8 pole double-winding BSRM as the research object, the solution formula for the slope range of stator pole helical teeth is derived. The torque change relationship of the motor is analyzed by finite element simulation, and the slope of the optimal result is 0.05. At this time, the torque ripple reduced by 32.5%, and the average torque increased by 26.7%, which provides a reliable method for optimizing the performance of the motor.*

**Keywords:** Bearingless switched reluctance motor, torque ripple, radial force, flywheel energy storage

## INTRODUCTION

Flywheel energy storage is a promising physical energy storage method, which is more friendly to the environment and has a longer service life than chemical energy storage. The working principle of flywheel energy storage is to achieve mutual conversion between kinetic energy and electrical energy by mutually driving between the flywheel rotor and the motor. Takemoto et al 1 established BSRM on the basis of SRM structure, BSRM used magnetic bearings instead of traditional mechanical bearings, and the proposal of magnetic bearing structure solved the problem of excessive friction loss of traditional mechanical bearings. With low loss and high efficiency, BSRM has become a popular motor for flywheel energy storage [2, 3]. Optimizing the torque performance of BSRM motor is of great significance to the long-term stable operation of motor and the practical application of flywheel energy storage. According to the literature [4] can be seen that the suspension winding providing magnetic bearing suspension force and the torque winding that provides rotor torque are highly coupled. The winding coupling will reduce the BSRM work efficiency. In order to solve the above problems, Bao Junfang et al. [5] proposed a new motor structure, the 12/14 pole BSRM structure is characterized by a non-uniform sub-pole arc structure. The torque pole with non-uniform stator arc structure realizes short magnetic circuit, and the torque and suspension force performance are analyzed, which proves that the structure has good decoupling characteristics. However, it is limited to the study of the structure of the motor body, and lacks the study of the suspension force and torque of BSRM. Sun Qin 6 researched a control strategy for better control of torque and suspension force.

*Author for Correspondence
Huiqin Sun
E-mail: shqczx@hebust.edu.cn

[1]Assistant Professor, School of Electrical Engineering, Hebei University of Science and Technology, China
[2]Student, School of Electrical Engineering, Hebei University of Science and Technology, China.

Received Date: September 05, 2022
Accepted Date: September 13, 2022
Published Date: September 30, 2022

**Citation:** Huiqin Sun, Sifei Wang, Wanqing Zhang, Chengran Mei, Zheng Tian, Chunzhi Shi. The Structure Optimization Design of Bearingless Switched Reluctance Motor for Flywheel Energy Storage. International Journal of Electrical Machines & Drives. 2022; 8(2): 1–11p.

 

Based on direct torque control, Direct Torque Control (DTC) and Direct Force Control (DFC) control strategies are put forward, and the mathematical model of motor in the non-overlapping section of stator and rotor teeth is expanded and analyzed. The mathematical model expands that application range of BSRM. In view of the problem that the instantaneous suspension force cannot be controlled when BSRM is running at high speed, Cao Xin et al [7] innovated the motor structure and designed a new 12/4 pole BSRM, which uses the motor structure to achieve sub-regional control of the suspension force and torque, and realizes natural decoupling. In order to improve the torque performance of BSRM, Yang Yan et al. 8 proposed a concentric magnetic gear with mixed magnetization. After comparison, it was found that, the output torque of BSRM under the gear structure was increased by 32%, and the optimization of the gear structure had certain reference value for optimizing the torque performance of the motor, but it was only suitable for the optimization of the low-speed motor structure. According to the above research content, the research on BSRM ontology design, control strategy, mathematical model and motor winding structure is relatively mature [4–8]. However, there is little research on the influence of BSRM stator teeth structure on torque and torque ripple.

In this paper, the purpose of reducing torque ripple is achieved by optimizing the structure of the bearingless switched reluctance motor. Firstly, the variables related to torque ripple are deduced, the formula for solving the minimum inclination of the helical teeth end of the stator is established, and the inclination range is determined. Secondly, in order to verify the accuracy of slope, the numerical simulation software ANSYS is used to simulate the radial force variation waveform and torque waveform under different slopes. Finally, by comparing the simulation results, the optimal stator skew angle is determined.

## THEORETICAL ANALYSIS OF BSRM

### Working Principle of BSRM

According to the literature [9], the structure of the 12/8 pole BSRM stator rotor is the same as that of the traditional 12/8 pole SRM stator rotor. The schematic diagram of the BSRM structure when phase A is on is shown in Figure 1. The number of turns of the main winding is Nm, and the current is ima. generates the torque force required for rotation of the drive motor. There are two sets of suspension windings in each phase, α the number of axial suspension winding turns is Ns1, the inflow current isa1, and the radial force affected by the two directions on the motor α shaft is different, so the radial suspension force of the α axis is generated; β axial suspension winding turns are Ns2, and the incoming current isa 2 will generate an axial suspension force of β. By controlling the positive and negative voltage and current size of the two sets of suspension windings, the rotor can be subjected to any direction and any size of suspension force, so that the radial suspension force overcomes the gravity of the rotor, and the magnetic levitation can be realized [10].

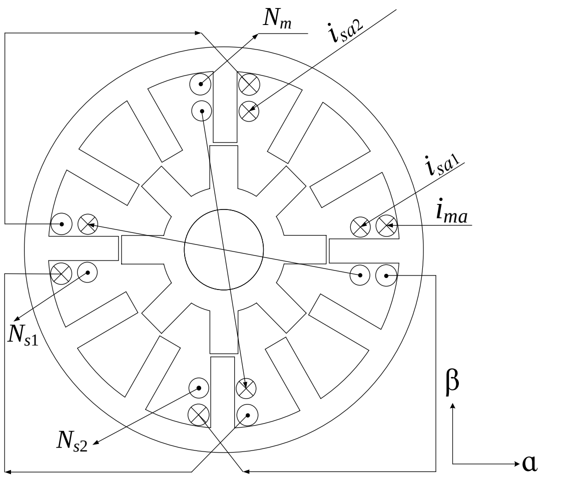


**Figure 1.** 12/8 Dual-winding BSRM structure when phase a is on.

 

When defining the rotor position angle, BSRM differs from SRM in that BSRM takes the position where the axis of the rotor teeth coincides with the center axis of the stator teeth as the zero-degree angle position [11]. The process from complete alignment of stator and rotor teeth to complete separation is defined as a conduction period.

**Parameters Affecting the Suspension Force and Torque Pulsation of BSRM**

The three-phase 12/8 pole BSRM follows the principle of three-phase rotational conduction, the magnetic common energy is represented by magnetic field energy storage when phase A is turned on 4, and the A-phase winding inductance matrix is introduced according to the equivalent magnetic circuit principle [12].

$$W_a = \frac{1}{2}[i_{ma} \quad i_{sa1} \quad i_{sa2}] \times [L] \times \begin{bmatrix} i_{ma} \\ i_{sa1} \\ i_{sa2} \end{bmatrix} \tag{1}$$

$$[L] = \begin{bmatrix} L_{ma} & M_{sma1} & M_{sma2} \\ M_{sma1} & L_{sa1} & M_{sa12} \\ M_{sma2} & M_{sa12} & L_{sa2} \end{bmatrix} \tag{2}$$

$L_{ma}$ is self-inductive for the main winding. $L_{sa1}$ and $L_{sa2}$ are suspension winding in α and β directions. $M_{sma1}$ and $M_{sma2}$ are the mutual inductance between the main winding and the floating winding in α and β directions respectively. $M_{sa12}$ is the mutual inductance between the suspension windings. Substitute (2) into the equation (1) obtainable equation (3).

$$W_a = \frac{1}{2}\left[{i_{ma}}^2 L_{ma} + {i_{sa1}}^2 L_{sa1} + {i_{sa2}}^2 L_{sa2} + 2 i_{ma} i_{sa1} M_{sma1} + 2 i_{ma} i_{sa2} M_{sma2}\right] \tag{3}$$

According to the principle of electromechanical energy conversion, when the A phase is conducted, the suspension force $F_\beta$ in the β direction, the electromagnetic torque $T_a$ such as equation (4), equation (5) can be found.

$$F_\beta = \frac{\partial W_a}{\partial \beta} \tag{4}$$

$$T_a = \frac{\partial W_a}{\partial \theta} \tag{5}$$

For easy calculation, suppose that the rotor position angle is 0°, at this time the air gap magnetic conductance of the four conduction positions of phase A is equal. $P_{ga1}$ is the air gap magnetic conductance in the positive direction of the β axis. $P_{ga2}$ is the air gap magnetic conductance in the direction of the negative α axis. $P_{ga3}$ is the air gap magnetic conductance in the direction of the negative β axis. $P_{ga4}$ is the air gap magnetic conductance in the positive direction of the α axis [13]. $P_{ga1}$=$P_{ga2}$=$P_{ga3}$=$P_{ga4}$, the mutual inductance between the windings is 0, according to the main and secondary winding self-inductance formula in the literature [4] the equation (3) is substituted for equation (4) and equation (5) respectively. Electromagnetic torque expression and β axis radial suspension force expressions such as equation (6), equation (8), $J_t(\theta)$ and $K_f(\theta)$ are respectively torque coefficient and suspension force coefficient.

$$T_a = J_t(\theta)(2N_m^2 i_{ma}^2 + N_{s1}^2 i_{sa1}^2 + N_{s2}^2 i_{sa2}^2) \tag{6}$$

$$J_t(\theta) = \left| \frac{\mu_0 hr}{l_g} - \frac{16\mu_0 chr}{\pi(\pi l_g - 4cr\theta)} \right| \tag{7}$$

$$F_\beta = K_f(\theta) N_m i_{ma} N_b i_{sa2} \tag{8}$$

$$K_f(\theta) = \left| \frac{\mu_0 hr(\pi - 12\theta)}{6 l_g^2} - \frac{32\mu_0 chr\theta}{\pi(\pi l_g^2 - 4crl_g\theta)} \right| \tag{9}$$

$\mu_0$ is 4π×10–7 H/m, which physically represents permeability of vacuum. $l_g$ represents the average length of the air gap. $h$ represents the axial length of the rotor. $\theta$ represents the rotor position angle. $r$

is the outer diameter of the rotor. $c$≈1.49 [2]. The torque performance of a motor is usually directly reflected by the torque ripple coefficient $m$ [14], which is defined as the ratio of the torque range to the average torque when the motor is running, as shown in equation (10).

$$m = \frac{T\text{min}_{max}}{T_{avg}} \tag{10}$$

From equations (6–9) can be seen, the number of turns of winding, motor parameters and air gap length are the main parameters affecting the motor torque and suspension force. As the motor structure and winding distribution have been set in the early stage of motor design, the fluctuation of the average length of air gap is the biggest influence on the torque ripple and suspension force of the motor. Reasonable optimization of the end structure of stator and rotor teeth can reduce the torque ripple caused by commutation.

## OPTIMIZE THE DESIGN OF BSRM

### Basic Parameters Design and Finite Element Analysis of Motor

BSRM parameter design can refer to the SRM motor design ideas [15]. The rated speed of high-speed motor for flywheel energy storage is usually not less than 10,000 rpm. In this paper, a three-phase 12/8 pole high-speed BSRM with rated power of 1.5 kW, rated voltage of 380 V and rated speed of not less than 15000 rpm is used for simulation. The specific parameters of the preliminary designed motor are shown in Table 1.

**Table 1.** Preliminary design motor parameters Table.

| Motor parameters | Value |
|---|---|
| Stator outer diameter | 145 mm |
| Stator inner diameter | 77 mm |
| Rotor outside diameter | 76.4 mm |
| Rotor inner diameter | 30 mm |
| Iron heart length | 90 mm |
| Constant/rotor polar aracari | 15° |
| Fixed/rotor yoke thickness | 9/14 mm |
| Primary/secondary winding | 22/18 circle |

In terms of air gap size, the air gap between stator and rotor of BSRM is slightly larger than that of ordinary SRM 16, which is to reduce the possibility of friction between the rotor and the auxiliary bearing due to vibration during the commutation of the BSRM. Therefore, the air gap is selected as 0.3 mm. The torque obtained from the preliminary design motor simulation is 0.9 N·m, the slot full rate is 45%, and the rated speed is 15224 rpm, which meets the motor design requirements.

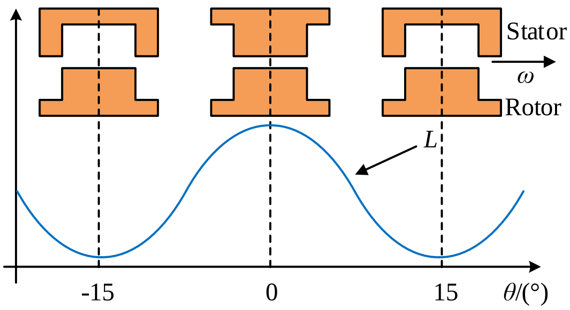


**Figure 2.** BSRM rotor position angle definition.

Based on the ANSYS-maxwell environment, the BSRM motor is modeled. Figure 3 shows the magnetic density diagram of the motor after the A phase suspension winding and the main winding are passed into 20A and 4A respectively. It can be seen from the Figure 2 that the magnetic flux in the positive direction of the β axis is 1.4T, the magnetic flux at the air gap in the negative direction of the β axis is 1.3T. The magnetic pulling force of the positive direction of β axis on the rotor is larger. Therefore, the motor generates radial suspension force in the positive direction of the β axis. The motor simulation experiment shows that the positive suspension force of β axis is 1500 N at this time. It can be seen from Figure 3 that at this moment, the radial suspension force of the α shaft of the motor is α the positive direction of the shaft, and the suspension force is 1500 N at this time.

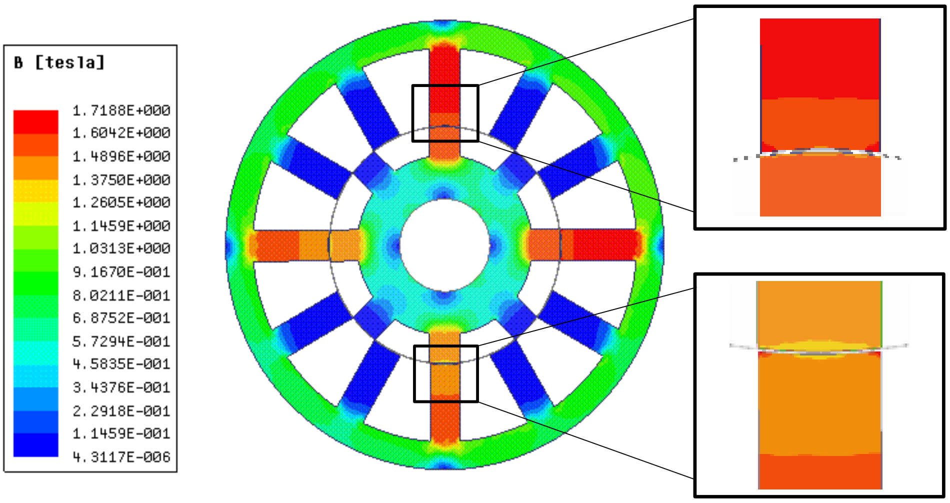


**Figure 3.** Air gap magnetic density diagram.

**Stator Teeth Optimization Design Scheme**

Switched reluctance motor torque is superimposed by a series of pulse torques, therefore, torque ripple is one of the disadvantages of BSRM [17]. By changing the structure of the motor body to optimize the change of air gap, the design stator pole helical teeth structure slope is $k$ see Figure 4, the magnetic flux path $P_2$ and $P_3$ parts of the motor air gap under this structure are still elliptical paths 18, and the $P_1$ part is no longer a uniform air gap length. The optimized average air gap length $l_g'$ is approximately expressed as equation (11).

$$l_g' = l_g + \frac{3.14kr(\pi+12\theta)}{12\pi} \tag{11}$$

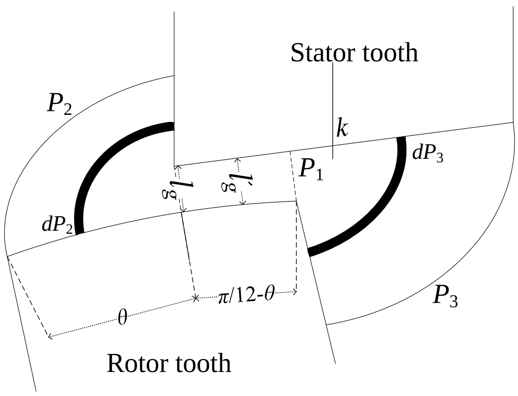


**Figure 4.** Exploded view of the air gap flux path after optimization.

The air gap range of the double convex pole motor specified in the project is 0.1 mm–1.0 mm. The minimum air gap $g_1$ between the rotor of the magnetic levitation motor and the auxiliary bearing is 0.25 mm. However, considering that the spiral teeth of the stator pole have a certain range of inclination in design, too large an inclination will lead to too large an average air gap, and the torque and suspension force will be reduced. According to this, the change of the distance between the motor rotor and the stator teeth when running is analyzed, and the stator tangent teeth slope solution equation is designed with the left teeth extreme point *D* point as the starting point, the coordinate of the *D* point is ($D_x$, $D_y$), and the inner diameter of the motor rotor is *R*.

$$\begin{cases} l_1: y_1 = k_1(x_1 + D_x) - D_y \\ l_2: (x_2 - O_x)^2 + (y_2 - O_y)^2 = R^2 \end{cases} \tag{12}$$

In equation (12), $l_1$ represents the straight line where the front of the stator pole helical teeth is located, the slope of the line is $k_1$. $l_1$ crosses the vertex $D(D_x, D_y)$ constantly. $l_2$ indicates the route of operation of the rotor teeth. The air gap distance $\triangle t(k, x)$ corresponding to $x_1$=$x_2$ is shown in equation (13).

$$\Delta t(k_1, x_1) = y_1 - y_2 = k_1(x_1 + D_x) \mp \sqrt{R^2 - (x_1 - O_x)^2} - O_x - D_y \tag{13}$$

$$\begin{cases} \dfrac{\partial \Delta_t(k_1,x_1)}{\partial x} = 0 \\ \Delta_t(k,x) = \Delta_t(k,x)_{min} \end{cases} = 0.25 \tag{14}$$

The *O* point is the motor center point with coordinates (0, 0), the motor *D* point coordinates are (-5.1, 38.25), and the motor rotor inner diameter *R* is 38.2 mm. Substitution (14) solves the system of equations and obtains two sets of solutions.

$$\begin{cases} k_1 = 0.0477 \\ x_1 = -1.8220 \end{cases} \qquad \begin{cases} k_2 = 0.2227 \\ x_2 = -8.3033 \end{cases}$$

Discard the solution with an inclination of 0.2227, when designing the helical teeth, the linear equation of the tooth end of the minimum slope helical tooth is $y = 0.0477x-1.822$. In order to make the average torque not much less than the torque target value, take the vertical distance between the end of the helical teeth and the rotor outer diameter movement trajectory is not more than 1.0mm. At this time, the maximum stator pole helical teeth inclination is 0.0689 according to the preliminary design size of the motor, and the optimal slope range of the stator pole helical teeth design of the bearingless switched reluctance motor is (0.05, 0.07) under the condition of meeting the requirements of the air gap design of the ordinary reluctance motor.

## SIMULATION ANALYSIS AND OPTIMIZATION DESIGN

### Comparison and Analysis of Radial Suspension Forces

When the three-phase 12/8 pole BSRM is running, the conduction law is A, B, C three-phase rotational conduction of 15° [19], BSRM suspension force fluctuations will also adversely affect the stable operation of the motor, two sets of suspension windings of BSRM generate α and β radial forces in two directions. Changing the stator structure will change the original air gap, and the change of air gap will have an impact on the magnetic field density, which in turn will change the radial suspension force of the motor. Therefore, when optimizing the motor, it is also necessary to take into account the variation waveform of radial suspension force of α and β axes. The end of the stator teeth is plotted in CAD, and the main and secondary winding currents are set to 20A and 4A respectively in the static field, and the suspension force changes are simulated in the A phase on-period as shown in Figure 5.

As can be seen from Figure 5, the greater the slope of the stator teeth, the greater the change in radial levitation force, which will increase the difficulty of control. According to the static field simulation results, the design range of stator pole helical teeth inclination derived from the theoretical air gap range is verified. When the inclination range of the stator skew teeth is (0.05, 0.07), the skew teeth structure will not reduce the average torque of the original motor, nor will it cause a big disturbance to the original suspension force of the motor, thus narrowing the simulation range of the subsequent motor optimization design.

 

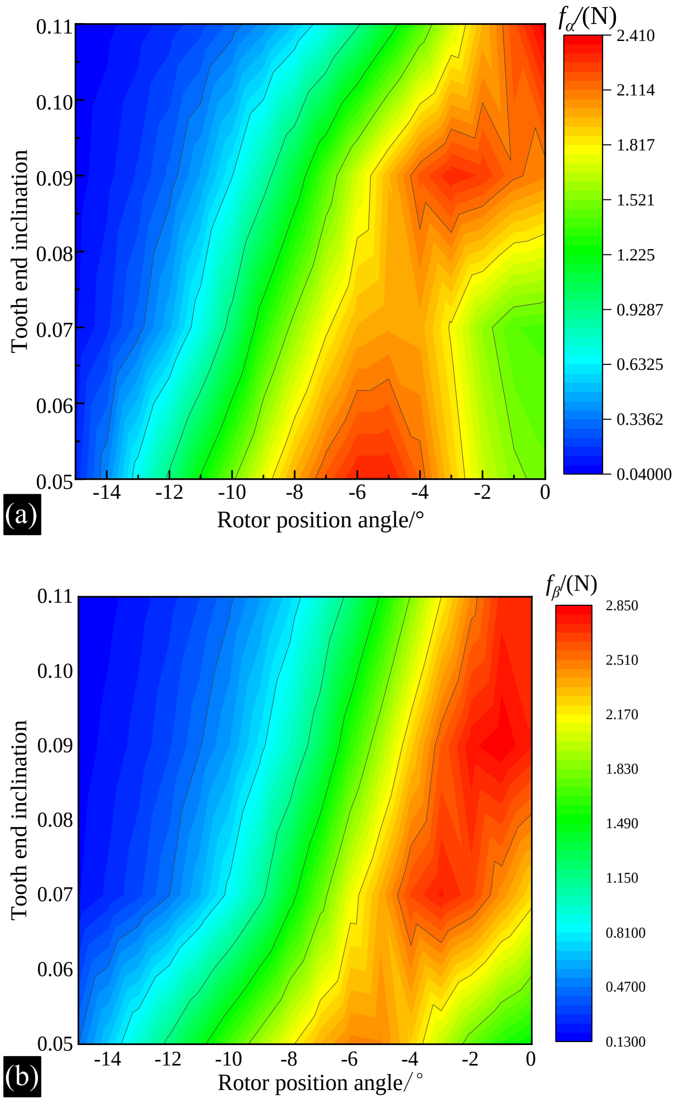


**Figure 5.** Variation of radial levitation force of a bearingless switching reluctance motor, (a) Comparison of radial suspension forces of α shafts, (b) Comparison of radial suspension forces of β shafts

**Torque Ripple Comparison and Analysis**

When the stator-helical teeth end slope is 0.05, 0.06 and 0.07, the torque during motor operation is simulated, and the simulation results of the motor torque performance parameters and the numerical change of torque ripple are shown in Figures 6 and 7.

It can be seen from Figure 6 that as the slope of the stator teeth end segment increases, the average torque of the motor as a whole shows an increasing trend. The maximum torque shows a decreasing trend. This is due to the fact that the helical teeth reduce the peak of the average air gap length of the Switched reluctance motor during operation, and the fluctuation of the air gap length change is smaller than before optimization, so the maximum torque optimization motor must not only reduce the torque ripple, but also meet the torque requirements of the motor design [20]. From Figure 7, it can be seen that the value of the motor torque ripple is 0.05 when the stator teeth slope is taken, the torque ripple is the minimum value, and the precision of the helical teeth is limited by the process manufacturing when the motor is manufactured, so this paper no longer does a more detailed simulation of the stator teeth slope, comprehensive consideration, the optimal stator teeth slope *k* determines to take 0.05.

 

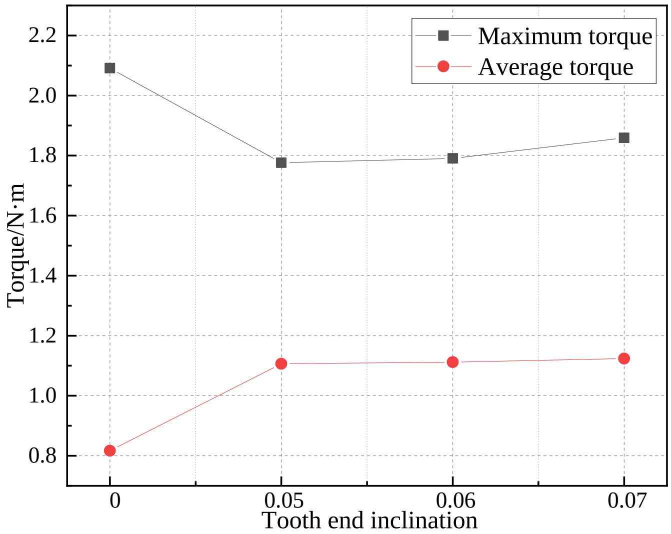


**Figure 6.** Torque change comparison chart.

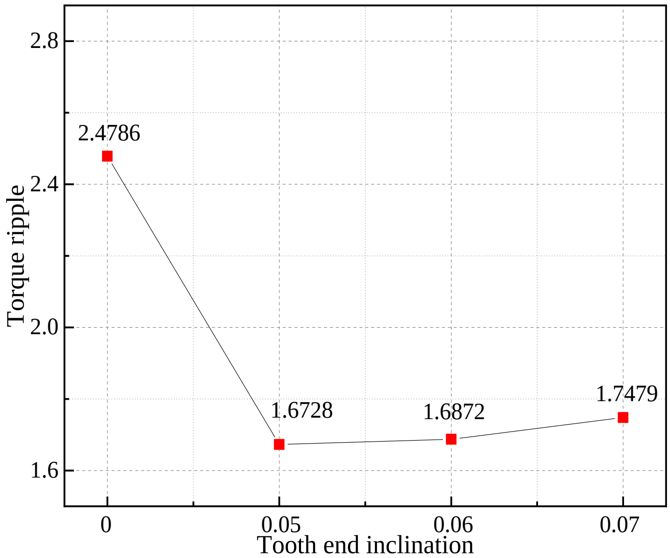


**Figure 7.** Torque ripple change graph.

**Optimize the Comparison and Analysis of Motor Performance Before and After**

Figure 8 is the motor output torque comparison chart before and after optimization, from the simulation data comparison can be obtained, the optimal stator teeth slope takes 0.05, the maximum torque of BSRM is reduced, for the high-speed motor applied to flywheel energy storage, the requirements for rotor speed are higher than the requirements for the maximum torque, the average torque of the motor after optimization increased from 0.86 N·m to 1.09 N·m, increased by 26.7%, and the torque ripple of the motor after the optimization of the figure analysis reduced by 32.5% compared with before optimization. The resulting motor performance is smoother after optimization.

When the rotor position angle is 0°, the air gap magnetic density curve of the motor obtained by the simulation before and after the optimization of the stator teeth is shown in Figure 9(a). The optimized stator teeth structure effectively reduces the edge flux effect and reduces the unnecessary air gap flux loss. The increase of radial magnetic density improves the suspension performance of the motor, and the suspension current can meet the suspension requirements of the motor within a small range of variation. Figure 9(b) shows a tangential air gap magnetic density waveform. Observing the change chart of tangential magnetic density, it can be seen that the end of the stator teeth is optimized, so that the air gap tangential magnetic density is unevenly distributed, which increases the maximum value of tangential magnetic density and has a favorable impact on increasing the average torque of the motor.

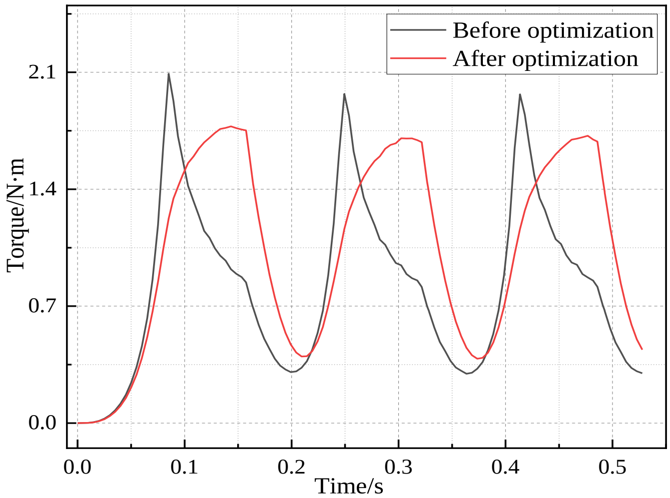


**Figure 8.** Optimized front and rear motor torque waveform comparison diagram.

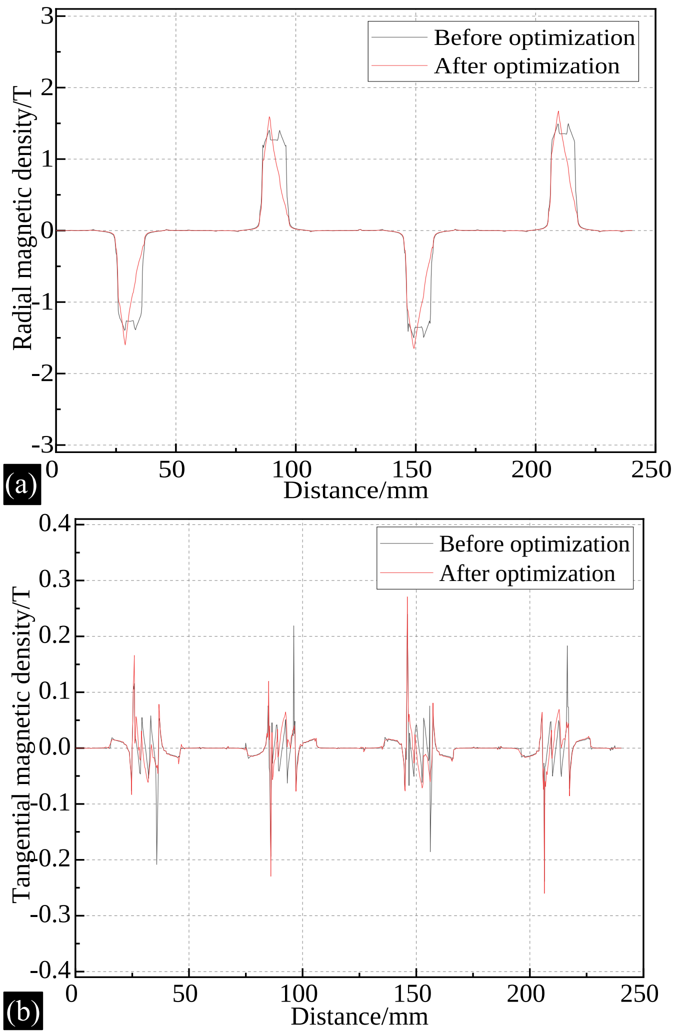


**Figure 9.** Comparison chart of air gap magnetic density of motor, (a) Radial magnetic density comparison, (b) Tangential magnetic density contrast

 

Optimize the torque performance of the motor, so that the motor torque in the commutation to reduce the fluctuation, reduce the difficulty of the follow-up control work, reduce the torque variable control range, stator pole helical teeth structure so that the motor radial suspension force changes, the corresponding theoretical suspension current waveform also needs to be adjusted, radial suspension force simulation for the motor based on the table method of direct suspension force control to provide reliable theoretical basis and data support.

## DISCUSSION AND CONCLUSION

In this paper, aiming at the situation that the torque ripple of high-speed BSRM for flywheel energy storage is large, the relationship between the torque and suspension force of BSRM motor and the air gap magnetic conductivity is derived from the equivalent magnetic circuit principle and the electromechanical energy conversion principle, and the structure of the stator teeth of the motor is changed, so that the fluctuation of the air gap change is reduced to reduce the torque ripple of the motor, and the design range of the stator teeth slope of the motor is given based on the design range of the engineering air gap design range. In order to verify the effectiveness of the stator helical teeth structure, an ANSYS simulation software was used to compare and analyze the torque performance of the motor under different stator helical teeth slopes. The main as follow:

1. Based on ANSYS software, a 12/8 dual-winding BSRM model was established in Maxwell-2D static field, and the electromagnetic simulation results of the motor proved the existence and controllability of the suspension force and verified the correctness of the model design.
2. Combined with the mathematical formula, the effect of the average air gap length on torque ripple and radial suspension force is verified, which provides more optimization ideas for optimizing the torque of the motor.
3. From the aspect of motor body design, an optimization scheme is proposed to reduce the torque ripple of BSRM, solve equality equation where the stator teeth of the simulation prototype are located, and give a solution method to calculate the optimization parameter range of the stator teeth slope, which improves the optimization efficiency and accuracy.

**Acknowledgment**

This research was supported by Hebei Provincial Science and Technology Plan (grant number 20314501D、19214501D).

## REFERENCES

1. Takemoto M., Shimada K., Chiba A, et al. A design and characteristics of switched reluctance type bearingless motors[C]//In Proc 4th Int Symp Magnetic Suspension Technology, May 1998: 49~63.
2. W Qi, Y. Mu, H. Wang, G. Zhou, et al. Design and analysis of improved bearingless switched reluctance motor for flywheel energy storage[C]//2021 China Automation Congress, 2021, pp. 5696–5700.
3. Y. Yuan, Y. Sun, Y. Huang. Design and analysis of bearingless flywheel motor specially for flywheel energy storage[J]. Electronics Letters, 2016, 52(1): 66–68.
4. J Z. Gao, Y.B. Liu, C.D. Zhou, et al. Magnetic circuit design and magnetic analytical model of permanent magnet suspension bearing for flywheel[J/OL]. Energy Storage Science and Technology. DOI:10.19799/j.cnki.2095–4239.2021.0485. (in Chinese)
5. J.F. bao, B.K. xue, S.F. tang, et.al. Design of new type 12/14 bearingless switched reluctance motor[J]. Electric Machines & Control Application, 2015,42(05):32–37+50. (in Chinese)
6. Q Sun. Optimization control of torque and radial force for dual-winding bearingless switched reluctance motor[D]. Nanjing University of Aeronautics and Astronautics, 2016. (in Chinese)
7. X cao, C.Y. liu, Z Q deng, et al. Decoupling mechanism and implementation of torque and levitation force in single-winding 12/4 bearingless [J]. Transactions of China Electrotechnical Society, 2018, 33(15):3527–3534. (in Chinese)
8. Y yang, X WU, P LI. Mathematical model of bearingless switched reluctance motors with double salient stators[J]. Small and Special Electrical Machines, 2017, 45(04):34–38. (in Chinese)

 

9. L. chen, H.H. wang, C tan. Innovative mathematical model for dual-winding bearingless switched reluctance motor based on Maxwell stress tensor method[J]. Electric Machines and Control, 2017, 21(11):9–18. (in Chinese)
10. Y.K. sun, B.B. zhang, Y yuan. Multi-objective optimal design of single winding bearingless switched reluctance motor for flywheel energy storage[J]. Electric Machines & Control Application, 2018, 45(10):53-58+119. (in Chinese)
11. F.X. huang. Design and analysis of bearingless switched reluctance motor for flywheel Battery[D]. Jiangsu University, 2020. (in Chinese)
12. Y.K. sun, J.B. wu, Q.W. xiang. The mathematic model of bearingless switched reluctance motor based on the finite-element analysis[J]. Proceedings of the CSEE, 2007(12):33–40. (in Chinese)
13. X. zhang, X.H. wang, Y B yang. The computation of vibration reduction capacity for switched reluctance motor based on improved magnetic field partition method[J]. Transactions of China Electrotechnical Society, 2015, 30(22):9–18. (in Chinese)
14. F F liu, Y yang, C W liu. Torque ripple study in bearingless switched reluctance motors with two different rotor's structure[J]. micromotors, 2016, 49(04):77–81. (in Chinese)
15. H.Q. sun, C cui, J W han, et al. Structure optimization design of switched reluctance motor based on air gap change[J]. micromotors, 2020, 53(10):5–10. (in Chinese)
16. J hu, C Y liu, Y yang. An automated determination method of convergent grid size based on ANSYS submodeling method[J]. Journal of Dalian Jiaotong University, 2019, 40(0257–60. (in Chinese)
17. W.Y. zou, Y.yang, Z.Y. liu, et al. Torque ripple control strategy for a 12 /8 single-winding BSRM with wider rotor teeth [J]. Small and Special Electrical Machines, 2020, 48(02):47–50+54. (in Chinese)
18. X cao, H.T. chen, Z.Q. deng. Analogy study of two types of multi degree of freedom switched reluctance motors[J]. Journal of Nanjing University of Aeronautics & Astronautics, 2020, 52(02):171–180. (in Chinese)
19. X.Y. chen. Mathematical model of bearingless switched reluctance motors with variable pole arc of stator and rotor teeth[J]. Small and Special Electrical Machines, 2013, 41(12):1–6. (in Chinese)
20. X zhang, X.H. wang, Y.B. yang, et al. Vibration reduction of a switched reluctance motor using new rotor tooth with slot on each side[J]. Proceedings of the CSEE, 2015, 35(06):1508–1515. (in Chinese)